

Mixing on the Late-Summer New England Shelf—Solibores, Shear, and Stratification

J. A. MACKINNON* AND M. C. GREGG

Applied Physics Laboratory and Department of Oceanography, University of Washington, Seattle, Washington

(Manuscript received 24 February 2002, in final form 3 December 2002)

ABSTRACT

Observations are presented of microstructure and velocity measurements made on the outer New England shelf in the late summer of 1996 as part of the Coastal Mixing and Optics Experiment. The depth- and time-averaged turbulent dissipation rate was $5\text{--}50 (\times 10^{-9} \text{ W kg}^{-1})$. The associated average diapycnal diffusivity in stratified water was $5\text{--}20 (\times 10^{-6} \text{ m}^2 \text{ s}^{-1})$, comparable to observed open-ocean thermocline values and too low to explain the strong variability observed in local water properties. Dissipation rates and diffusivity were both highly episodic. Turbulent boundary layers grew down from the surface and up from the bottom. The dissipation rate within the bottom boundary layer had an average of $1.2 \times 10^{-7} \text{ W kg}^{-1}$ and varied in magnitude with the strength of near-bottom flow from the barotropic tide, an along-shelf flow, and low-frequency internal waves. The average dissipation rate in the peak thermocline was $5 \times 10^{-8} \text{ W kg}^{-1}$; one-half of the thermocline dissipation was due to the strong shear and strain within six solibores that cumulatively lasted less than a day but contained 100-fold elevated dissipation and diffusivity. Nonsolibore, midcolumn dissipation was strongly correlated with shear from low-frequency internal waves. Dissipation was not well parameterized by Gregg–Henyey-type scaling. An alternate scaling, modified to account for observed coastal internal wave properties, was in good agreement with measured dissipation rates. At the end of the observational period Hurricane Edouard passed by, producing strong dissipation rates ($4 \times 10^{-6} \text{ W kg}^{-1}$) and consequent mixing during and for several days following the peak winds.

1. Introduction

The Mid-Atlantic Bight continental shelf is a diverse environment, where local physical processes are key to understanding optical properties, small-scale biology, and sediment movement. Diapycnal mixing may be a vital mechanism controlling the distribution of physical water properties, nutrient fluxes, and concentrations of particulate matter. The outer shelf south of New England provides a forum in which to examine levels of shelf mixing and explore the physical processes that determine those levels and variability.

Mooring measurements made as part of the Coastal Mixing and Optics (CMO) Experiment reveal a strong seasonal cycle in external forcing and water properties (Gardner et al. 2001). To first-order, shelf water is well mixed by strong surface wind forcing during the winter. From late spring to late summer, stratification created by local heating and freshwater advection limits the vertical extent of surface and bottom boundary layers and allows a large “midcolumn” vertical range in which turbulent fluxes are controlled by internal wave insta-

bilities. The goal of this study is to delimit the relative roles of boundary friction and internal wave dynamics in generating turbulent fluxes through stratified water on the late-summer shelf. We focus on understanding the patterns of turbulence away from boundaries, the dynamical relationships between this turbulence, internal-wave shear and stratification, and the applicability of parameterizations that have been successfully used to relate turbulence and internal wave instabilities elsewhere in the ocean. MacKinnon and Gregg (2003b, manuscript submitted to *J. Phys. Oceanogr.*) present a parallel analysis of turbulence measurements taken at the other end of the stratified season, during the following spring restratification.

Turbulent dissipation has been well studied and typified in many parts of the world (Gregg 1998; Polzin et al. 1995). Diapycnal diffusivity from turbulent mixing in the open ocean thermocline ranges from 5×10^{-6} to $3 \times 10^{-5} \text{ m}^2 \text{ s}^{-1}$. It is elevated several orders of magnitude above this in the presence of mesoscale features such as fronts and rings, and over irregular topography. Gregg (1989, 1998) and Polzin et al. (1995) suggest that a first-order understanding has been achieved relating turbulence to local stratification and the energy level and spectral properties of internal waves. Specifically, the most successful models assume that the rate of turbulent energy dissipation is controlled

* Current affiliation: IOD/SIO, La Jolla, California.

Corresponding author address: Dr. J. A. MacKinnon, IOD/SIO, 9500 Gilman Drive, Mail Code 0209, La Jolla, CA 92093-0209.
E-mail: jen@coast.ucsd.edu

by the rate of spectral energy transfer from large to small scales through wave–wave interactions in a steady-state, broadband, internal wave field. One of the main goals of this paper is to evaluate to what extent successful wave–wave interaction models of turbulence apply on the continental shelf.

Comparatively little work has been done to assess mixing on continental shelves. There are myriad reasons why turbulence on shelves is likely to differ from that in the open ocean: boundaries are never far away; strong and variable lateral gradients in water properties are often present; timescales of wave forcing are comparable to the timescales of wave dissipation; and the internal wave field, dominated by low-mode, narrowband waves, is rarely in steady state.

Several studies have suggested that boundary effects dominate turbulence in shallow environments, especially when stratification is weak. For example, Simpson et al. (1996) and Simpson et al. (2000) observe strong turbulence rising off the bottom in the Irish Sea, consistent with simple analytical and numerical models of tidal friction. Inall et al. (2000), working on the Malin shelf, show that over half the observed dissipation is in the bottom boundary layer. Nash and Moum (2001) find strong dissipation on the Oregon continental shelf in a region of hydraulic control near the bottom.

On the other hand, Simpson et al. (1996), Inall et al. (2000), and Rippeth and Inall (2002) discover strong turbulence in the thermocline that is inconsistent with generation by surface or bottom stresses. Inall et al. (2000) make a convincing qualitative argument for a causal relationship between enhanced thermocline dissipation and strong shear from a nonlinear internal tide. Earlier work by Sandstrom and Elliot (1984) and Sandstrom and Oakey (1995) on the Scotian shelf showed that a significant portion of the amplitude loss experienced by internal solitary waves propagating upshelf was due to turbulent dissipation in a thin pycnocline.

Here we present basic observations of physical conditions on the later summer shelf and a detailed geography of observed mixing. A thorough discussion of the local wavefield, associated shear and calculated energy fluxes is presented in a companion paper, MacKinnon and Gregg (2003a, hereinafter referred to as MGa). Section 2 describes our instruments and measurement techniques. We present an overview of the background physical conditions at our observation site that provide the context for our dissipation observations in section 3. Section 4 begins with an overview of mixing on the shelf, including average levels of dissipation and diffusivity. We then investigate specific areas of mixing during the first two weeks of the cruise. In section 5 we discuss mechanisms of mixing on the shelf, focusing primarily on parameterizations of stratified mixing. We discuss the effects of observed turbulence and compare our results with other measurements in section 6. A summary of our results is presented in section 7.

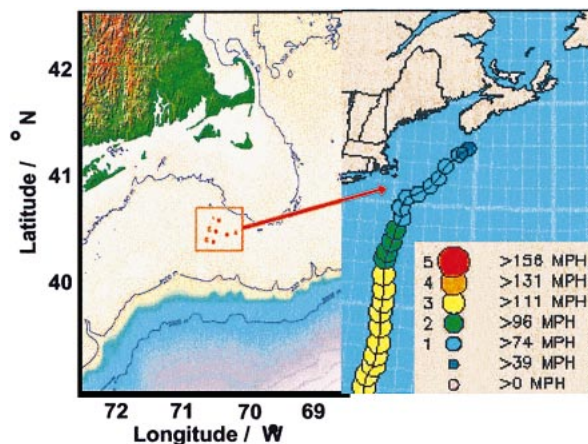


FIG. 1. Location of the CMO experiment (square in left panel). Profiling took place near the central site (labeled “C”) in a box 1.5 km wide (not shown). The right panel represents the path and changing wind speed of Hurricane Edouard in early September. (Panels are at different scales.) The arrow between panels indicates the rough location of the CMO site. Right panel courtesy of S. Babin and R. Sterner, The Johns Hopkins University Applied Physics Laboratory.

2. Experimental methods

a. Experiment

From 19 August to 1 September 1996, we obtained microstructure, velocity, and echosounder data on the New England Shelf on board the R/V *Seward Johnson* near the 70-m isobath south of Nantucket in a region known as the “mud patch” for its small sediment size (Fig. 1). The vessel steamed slowly east and west (to prevent the profiler from moving under the ship) in a box 1.5 km along-shelf and 1 km across-shelf centered near 40°30′N, 70°30′W. On 1 September the ship was forced into port due to the imminent arrival of Hurricane Edouard. We returned to the site 4 September and completed two more nights of profiling in posthurricane conditions. Here we treat our observations as occurring in a fixed location. However, some water property gradients within the profiling box were apparent. While this aliasing does not change any fundamental results, it highlights the complexity of the shelf and the importance of advection. The date convention used is that noon on 1 January is yearday 0.5.

b. Microstructure

Our primary instrument was the Modular Microstructure Profiler (MMP)—a loosely tethered, free-falling instrument ballasted to fall at 0.5 m s^{-1} . We generally worked in 12-h shifts at night. We completed a full water column profile approximately every 4 min during peak operating efficiency, resulting in 1469 total profiles before the hurricane and 1698 overall. The MMP is equipped with SeaBird temperature and conductivity sensors, two airfoil probes, an optical backscatter sensor, and a small acoustic altimeter. Using the altimeter, we

were able to monitor the instrument location and safely profile to within a few meters of the bottom. The airfoils measured high-frequency velocity fluctuations, which were used to calculate the local rate of turbulent dissipation ϵ (Oakey 1982; Wesson and Gregg 1994). Dissipation measurements were unreliable in the top several meters because of contamination by the ship's wake and above 8 m because of strong tilting of the profiler. In stratified water diapycnal diffusivity was calculated based on an assumed relationship with turbulent dissipation and stratification, $K_p \leq 0.2\epsilon/N^2$ (Osborn 1980). Though MMP quantities are measured as a function of pressure, here all quantities are plotted versus depth for comparison with ADCP data; this approach results in an average error of less than 1%.

c. Velocity

We obtained continuous time series of velocity at 1-min intervals and 4-m vertical spacing between 8 and 56 m from two shipboard broadband ADCPs. From these data we calculated barotropic (depth mean) and baroclinic (depth mean removed) velocities as well as shear (first-differenced velocity). Velocity data during the hurricane were measured by a mooring 1 km away from our site and are presented here courtesy of researchers at Oregon State University (O'Malley et al. 1997). Further details of velocity and shear analysis are described in MGa.

3. Shelf environment

a. Meteorological conditions

Weather on the shelf before Hurricane Edouard was dominated by sunny days and warm nights with light winds. Net surface buoyancy flux (into the ocean) and wind stress were measured by a Woods Hole Oceanographic Institution meteorological mooring (data courtesy of S. Lentz, S. Anderson, J. Edson, and A. Plueddemann). During nighttime profiling periods heat loss to the atmosphere produced a buoyancy flux of 3–8 ($\times 10^{-8} \text{ W kg}^{-1}$). Wind stress was less than 0.15 N m^{-2} until the arrival of Hurricane Edouard. On 2 September the eye of the hurricane passed within 110 km and local wind speeds reached 20 m s^{-1} (Dickey et al. 1998). On 4 September when profiling recommenced, both surface wind stress and nighttime buoyancy flux had returned to prehurricane values.

b. Water properties

1) PREHURRICANE EVOLUTION

Water on the shelf is cooler and fresher than the adjoining Atlantic, leading to a strong shelfbreak front that is the most notable hydrographic feature in this region. The front extends seaward from a foot usually located near the 85-m isobath, about 20 km south of our site

(Linder and Gawarkiewicz 1998; Barth et al. 1998). Previous studies have concluded that shelf water is primarily traveling south along isobaths, originating north of the Scotian shelf (Chapman and Beardsley 1989). Local spring and summer warming contribute to a strong thermocline overlaying a cold pool of remnant water from the previous winter's mixing (Chapman and Beardsley 1989; Houghton et al. 1982).

Typical profiles of salinity, temperature, and density from the microstructure profiler are shown in Fig. 2a. A corresponding profile of buoyancy frequency is shown in Fig. 2b. The stratified interior was typically bounded on the top and bottom by well-mixed layers. We define the surface (bottom) mixed layer as that region with density within 0.01 kg m^{-3} of the smallest (largest) density (Fig. 2). Average surface and bottom mixed layer heights were 5 and 10 m, respectively.

There were substantial advective water property changes at all depths before the hurricane. The clearest signal of advection was the changing potential density of the deepest water, which ranged from 25.1 to 25.6 kg m^{-3} , consistent in magnitude with advection of across- and along-shelf gradients (Fig. 3). Changes in temperature and salinity on an isopycnal surface are often indicators of advective change. The most dramatic isopycnal water property excursion was a large intrusion of warm salty water at middepth on yeardays 238 and 239 (Gardner et al. 2001). Overall, isopycnal temperature and salinity fluctuated on timescales of hours to days, with standard deviations of 0.18°C and 0.05 psu, respectively. Previous studies have concluded that both across-shelf and along-shelf advection are important in this area (Voorhis et al. 1976).

Patchy and variable stratification provided a changing environment for local internal waves and turbulence. Figure 4a shows a complete record of stratification evolution. On a daily basis, low-mode internal waves produced thermocline displacements of 5–15 m (Figs. 3 and 4a, MGa). This isopycnal heave effectively smeared the strong thermocline (as well as strong vertical structure in other variables) in an isobaric average (Fig. 5a). Hence we also compute averages of stratification and other properties along isopycnal surfaces, taking care to weight equal volumes of water equally (Figs. 5d–f). Below the thermocline, there were numerous patches 5–10 m high of well-mixed water away from boundary layers (e.g., Fig. 2 and Fig. 4a near 50 m on yeardays 240, 241, and 242). These patches may be detached bottom mixed layers from farther upshelf.

Local stratification changes also reflected the larger-scale density field evolution, as the relative spacing of isopycnals across- and along-shelf evolved (J. Barth 2001, personal communication; Barth et al. 1998). For example, the dense foot of the front was closer to our position on yeardays 242 and 243, which corresponded to a compression of isopycnals and an increase in stratification between the thermocline and the bottom boundary layer (Figs. 3, 4a).

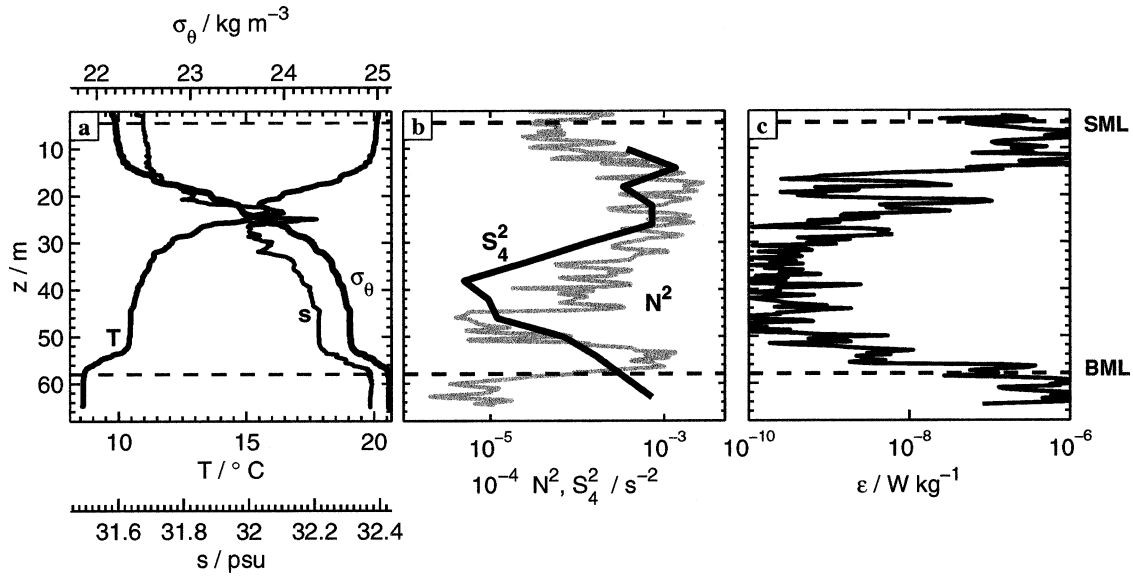


FIG. 2. (a) Typical profiles of potential temperature, salinity, and potential density; (b) shear (black) and stratification (gray); (c) dissipation rate. The lowest and highest horizontal dashed lines in each panel represent the edges of the bottom and surface mixed layers. The profiles were taken on yearday 236.17.

2) POSTHURRICANE CONDITIONS

The water column became significantly less stratified during the passage of Hurricane Edouard, and continued to adjust throughout the two nights of posthurricane profiling (Fig. 3). WHOI and Oregon State University moorings provided continuous records of wind stress, water temperature, and velocity during the hurricane (Fig. 6). During and immediately following the storm, the surface layer mixed downward, while the bottom layer mixed upward more slowly (Dickey et al. 1998). By yearday 247 the water had a clear two-layer structure with a strongly stratified (16 cph) interface between 35 and 50 m and a surface cap of warmer fresher water (Figs. 4a, 7). The total density range was reduced to less than one-third its prehurricane value (Figs. 3 and 7). Depth-integrated heat and salt were conserved, con-

sistent with local mixing of the prehurricane shelf water. Over the course of the following day (yearday 248), the water became more continuously stratified, while the total density range continued to drop (Fig. 7).

c. Energy and shear

Water motion on the summer shelf primarily consisted of an along-shelf mean flow, a mixed barotropic tide, low-frequency, low-vertical-mode internal waves, and occasional energetic internal solibores. Energy and shear before the hurricane are discussed extensively in MGa. Their major results are summarized as follows:

- Baroclinic energy on the summer shelf was primarily composed of low-mode, near-inertial and semidiurnal internal waves. Throughout MGa and here, the term

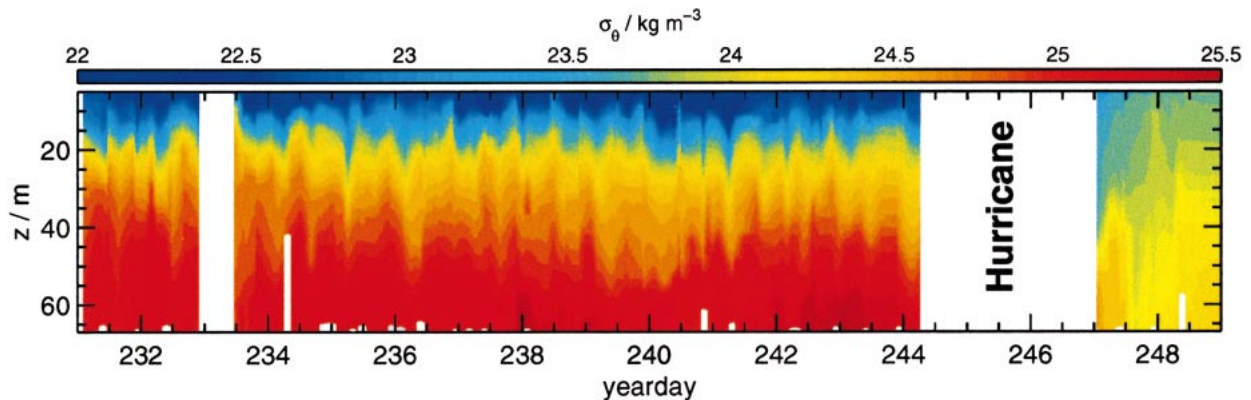


FIG. 3. Potential density evolution. Data have been filtered and subsampled to 2-h intervals during the nights. Density measurements during the daytime are reproduced with permission from Gardner et al. (2001).

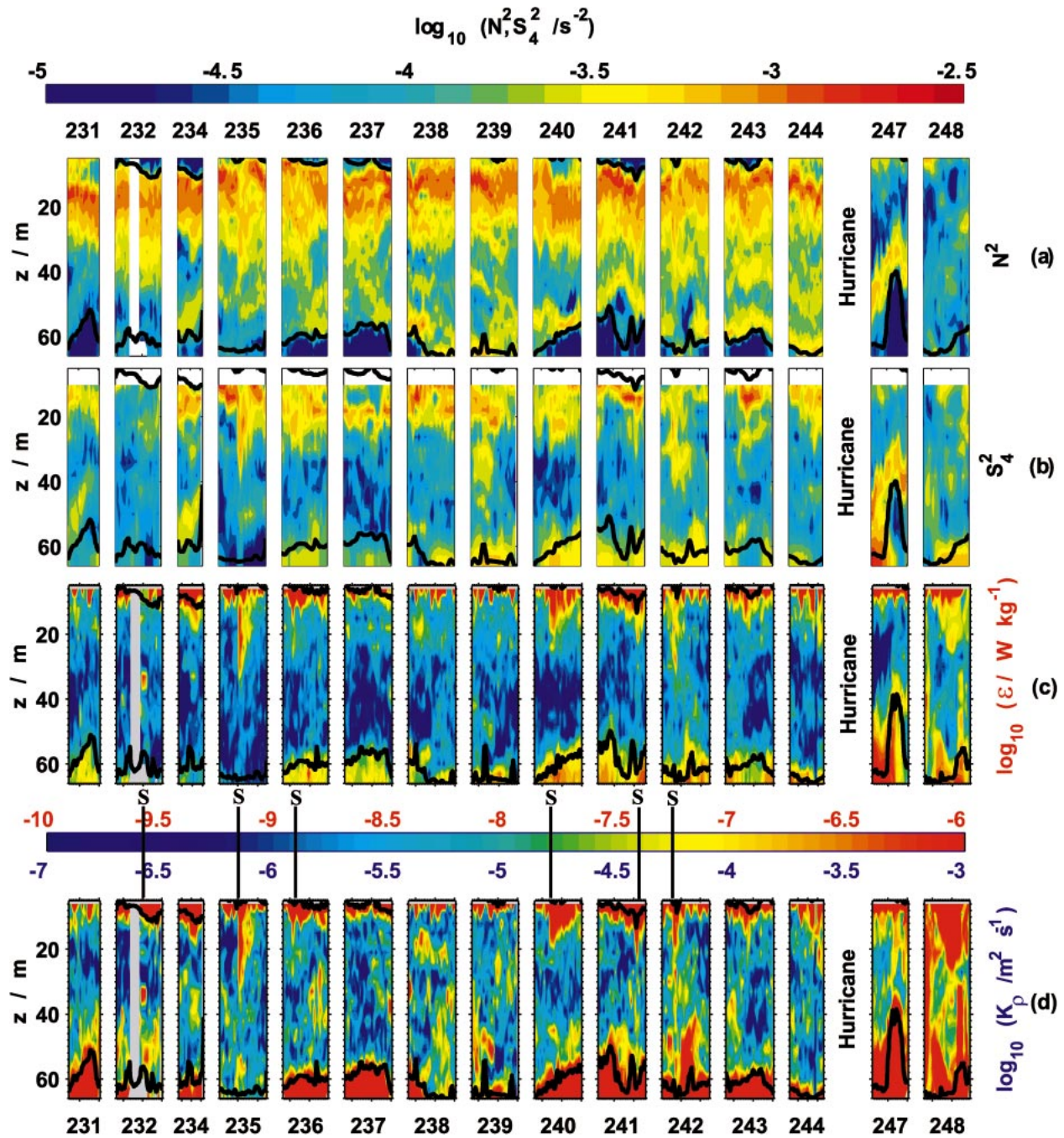


FIG. 4. (a) Buoyancy frequency. (b) Four-meter shear variance from shipboard ADCPs; the deepest value was based on a linear extrapolation of the deepest velocity measurement to a no-slip boundary condition. (c) Turbulent dissipation rate. (d) Diapycnal diffusivity. Data for (a), (c), and (d) have been smoothed to 2.5-m and 30-min resolution. Data in (b) have 4-m and 30-min resolution. The thick black lines indicate the boundaries of surface and bottom mixed layer. Each solibore is indicated with an “S”. All data are shown only during microstructure profiling periods; the gaps between panels are not to scale.

low-frequency refers to velocity and shear data that have been low-passed below 0.17 cph. Both the total energy and the relative energy from distinct vertical modes fluctuated by an order of magnitude over the fortnight of observations. There was little correlation

between the energy of low and high vertical-mode waves.

- Shear variance changed in response to both changing energy and changing relative modal content. During periods of high-mode waves (e.g., yeardays 237–239),

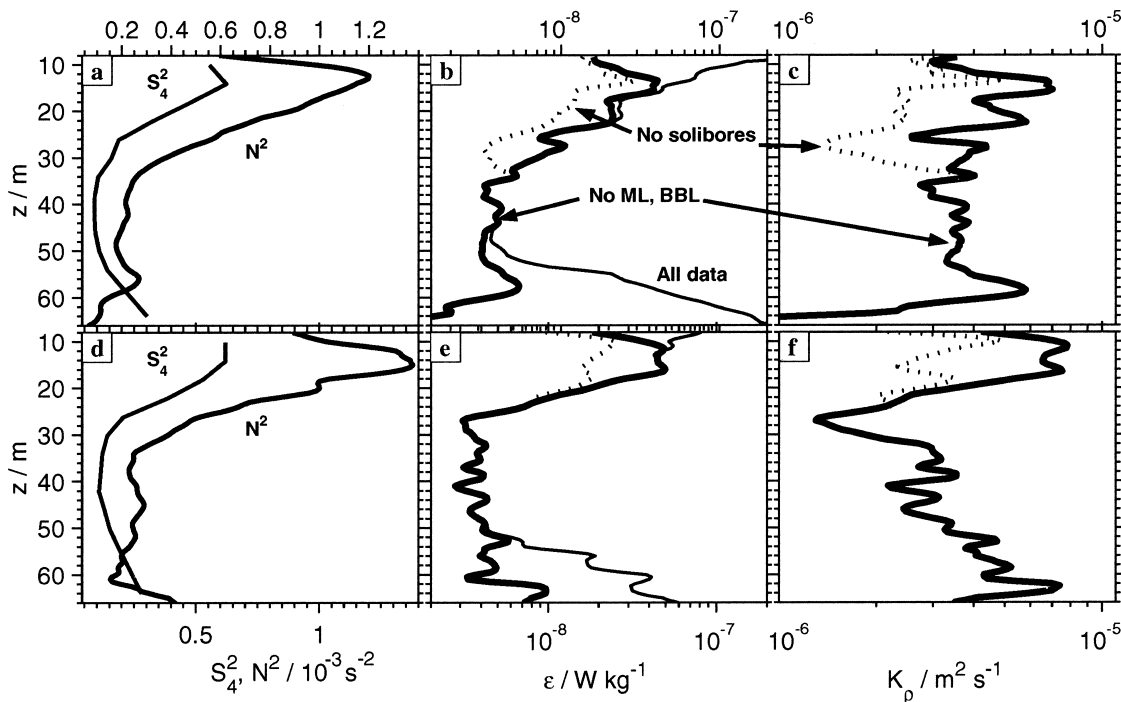


FIG. 5. Top: isobaric averages of (a) stratification and shear, (b) dissipation rate, and (c) diapycnal diffusivity. Bottom: isopycnal averages of the same quantities. For dissipation, (b) and (e), the thin solid lines include all data before the hurricane, the thick solid lines exclude the surface and bottom boundary layers, and the dotted lines further exclude the solibores. Because diffusivity is not well defined in mixed layers, we do not include the full (thin solid) averages in (c) and (f).

shear was relatively large (compared to energy), and spread out over a range of depths below the thermocline.

- Energetic, high-frequency solibores episodically passed through the CMO site, producing large vertical displacements and high shears that at times lowered the 4-m Richardson number below the threshold for shear instability. The term solibore refers to high-frequency, large amplitude internal waves that have both soliton and bore-like characteristics (Henyey and Hoering 1997).

Hurricane Edouard greatly elevated kinetic energy, near-bottom shear, and to a lesser extent midcolumn shear during and for several days after its closest approach. During the strongest hurricane winds, velocity fluctuations were extreme and kinetic energy increased substantially (Fig. 6b). After the hurricane passed, the barotropic energy continued to rise as the along-shelf flow sped up, peaking above 0.4 m s^{-1} near yearday 248, before gradually returning to its prehurricane speed by yearday 252. The barotropic tide, which appeared to be primarily diurnal following the hurricane, alternately flowed with and against the along-shelf mean flow to produce large fluctuations in total barotropic energy (Fig. 6b).

The average baroclinic energy during the two days after the storm passage was $7.4 \times 10^{-3} \text{ J kg}^{-1}$, 1.5 times the prehurricane average. By yearday 247, when pro-

filings recommenced, the baroclinic velocity was dominated by a semidiurnal internal tide with a two-layer vertical structure that mirrored the two-layer density structure. The density interface moved upward with the internal tide over the course of the night (Fig. 4a). Peak shear followed the interface movement (Fig. 4b) and ranged from 5 to $15 (\times 10^{-4} \text{ s}^{-2})$. As the water column became more continuously stratified on yearday 248, shear became more evenly distributed throughout the water column. On both nights of profiling the average 4-m Richardson number in stratified water was order unity, close to the threshold for shear instability.

d. Strain

Other investigators (Kunze et al. 1990; Wijesekera et al. 1993; Alford and Pinkel 2000) report strain to be dynamically relevant to turbulence. However, strain did not play a dominant role for the low-frequency waves observed here. The near-inertial waves that we observed were close to the lower frequency limit of the internal wave band; hence vertical displacements were small. Vertical displacements associated with the slightly higher-frequency, semidiurnal waves were on the order of 5–10 m (Fig. 3) and were largest in the thermocline. Strain, the vertical divergence of vertical displacement, had the same vertical structure as horizontal velocity, with a minimum in the thermocline for a mode-1 stand-

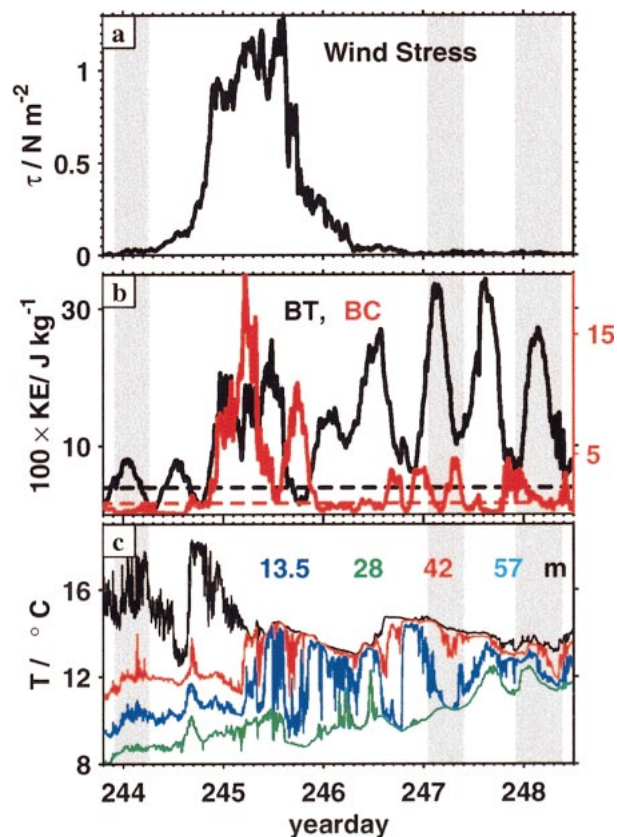


FIG. 6. (a) Wind stress during and after the hurricane passage. (b) Barotropic and baroclinic energy. (c) Temperature at 13.5, 28, 42, and 57 m. The shaded areas indicate profiling periods. Wind stress data courtesy of S. Anderson, J. Edson, A. Plueddemann, and S. Lentz (all at WHOI) as well as ONR. Temperature data and energy during the hurricane courtesy of OSU.

ing wave. For example, vertical displacements from the internal tide on yearday 231 ranged from 0 at 5-m depth to 5-m displacements at 20-m depth, producing a strain of 0.3. Peak strain and peak shear are vertically out of phase in standing waves, and hence do not combine to reduce Richardson numbers as efficiently as they do for freely propagating waves (Kunze et al. 1990). Strain may be dynamically important during solibores (MGa). Otherwise, it was virtually impossible to measure strain over short times and small vertical scales, as density changes on these scales were dominated by horizontal advection [see section 3b(1)].

4. Mixing levels on the shelf

Dissipation and mixing on the shelf were mainly controlled by near-bottom friction and shear from low-frequency internal waves and solibores, except during the hurricane. Contoured dissipation rates and associated diapycnal diffusivities for each night of profiling are shown in Figs. 4c and 4d, where boundaries of surface and bottom mixed layers are overlain. Most of the dis-

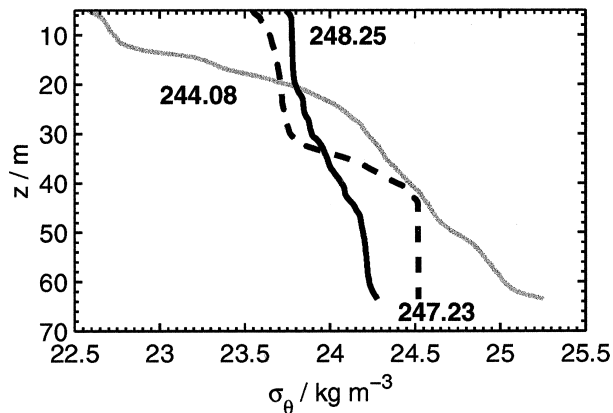


FIG. 7. Typical potential density profiles from before (yearday 244.08, gray line) and after the hurricane (yearday 247.23, dashed; yearday 248.25, solid). The two posthurricane profiles were taken at similar phases of the semidiurnal tide.

sipation occurred near the bottom, in relatively well-mixed water (Fig. 4c). The largest buoyancy fluxes were in the stratified region just above the bottom mixed layer and in patches concentrated near the thermocline. Several of these patches (labeled with an “S” in Fig. 4) were particularly strong and coincided with solibores. Diffusivity was also patchy, though the patches were more evenly spread throughout the water column (Fig. 4d).

The average vertical structures of prehurricane dissipation rate and diffusivity are shown in Fig. 5. The top panels represent isobaric averages, while the bottom panels represent averages taken along isopycnals, plotted versus the average depth of each isopycnal. To elucidate the role of different dynamical processes, average dissipation rate profiles based on three subsets of the prehurricane data are presented: all data, data without boundary layers, and data excluding both boundary layers and solibores (Figs. 5b and 5e). The boundary layers dominated dissipation in the top 15 m and the bottom 20 m. When boundary layers were excluded from consideration, 75% of dissipation was located in the thermocline, half of which occurred during solibore passage.

Average diffusivity profiles were calculated from averages of dissipation rate and stratification. Because diffusivity was not well defined in the well-mixed boundary layers, average diffusivity profiles are only shown for data excluding the boundary layers and data further excluding the solibores (Figs. 5c and 5f). The average diffusivity associated with midcolumn, stratified turbulence was $5 \times 10^{-6} \text{ m}^2 \text{ s}^{-1}$, comparable to levels in the open-ocean thermocline (Gregg 1998; Polzin et al. 1995; Ledwell et al. 1993). The average thermocline diffusivity was also dominated by a few solibores, especially when computed isopycnally (Fig. 5f). In the remainder of this section, we investigate the magnitude and variability of the primary shelf mixing processes in more detail.

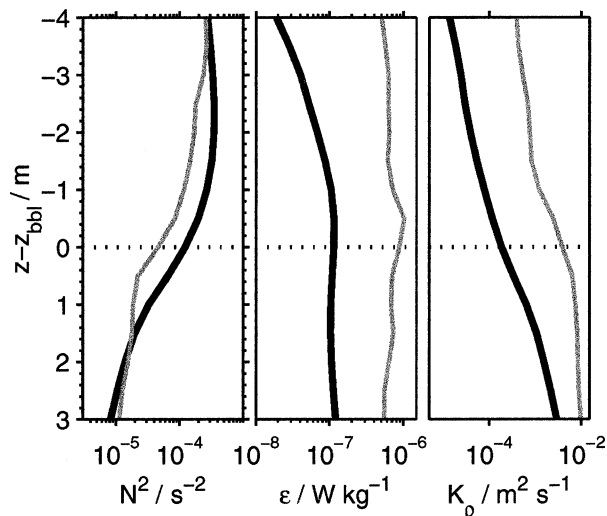


FIG. 8. Average stratification, dissipation, and diapycnal diffusivity computed in a frame of reference that moves with the bottom mixed layer height from before (thick black) and after (thin gray) the hurricane.

a. Boundary layer mixing

Over one-half of the observed energy dissipation and some of the strongest buoyancy fluxes on the shelf occurred in the bottom boundary layer. During the fortnight before the hurricane, 55% of the observed dissipation occurred in the unstratified bottom mixed layer or in an actively dissipating stratified entrainment zone just above it. The magnitude of dissipation was well correlated ($R = 0.87$) with the current speed at 56 m. To accurately predict or model the evolving bottom dissipation and energy loss, it is essential to understand the variability of near-bottom barotropic and baroclinic flow (MGa). For example, at times when the barotropic and baroclinic flow destructively combined to produce negligible near-bottom currents, boundary-layer dissipation waned (Fig. 4c, yearday 235).

In order to measure fluxes through the top of the bottom mixed layer, the height of which (advectively) changed by a factor of 2 on a daily basis, we computed averages of dissipation, stratification, and diffusivity in a frame of reference that moved with the bottom mixed layer top (Fig. 8). Average prehurricane diffusivity in the stratified mixed layer cap was $10^{-4} \text{ m}^2 \text{ s}^{-1}$. The average buoyancy flux through the stratified top of the boundary layer, $J_B = K_\rho N^2$, was $2 \times 10^{-8} \text{ W kg}^{-1}$.

After the hurricane, strong currents and reduced stratification allowed stronger boundary-layer turbulence. During yearday 247 almost all the dissipation occurred below the interface separating two relatively well-mixed layers (Fig. 4). Dissipation throughout this area began strong ($\epsilon > 1 \times 10^{-6} \text{ W kg}^{-1}$) and extended in a near-continuous patch from the bottom through the stratified interface. As the tide turned against the mean along-shelf flow, current speed dropped from 0.7 to 0.2 m s^{-1}

and dissipation dropped several orders of magnitude (Fig. 4c). Higher posthurricane dissipation resulted in larger average diffusivity through the top of the bottom mixed layer than was observed before the hurricane (Fig. 8).

Dissipation within the shallow surface boundary layer was not usually within the depth range of reliable microstructure measurements. With light winds and small nighttime buoyancy fluxes, we did not expect large near-surface dissipation rates before the hurricane. From our limited near-surface data we measured an average dissipation in the surface mixed layer of $5 \times 10^{-7} \text{ W kg}^{-1}$. Average dissipation and diffusivity in the stratified entrainment zone at the bottom of the surface mixed layer were $2 \times 10^{-7} \text{ W kg}^{-1}$ and $4 \times 10^{-5} \text{ m}^2 \text{ s}^{-1}$.

b. Midcolumn mixing

Midcolumn, nonsolibore mixing was strongly concentrated in the thermocline and correlated with the evolving shear field. Average profiles of stratification, shear, and nonsolibore dissipation all peaked between 10 and 15 m and declined steadily with depth (Figs. 5a and 5b). Isopycnal averages were more strongly concentrated, suggesting that high dissipation and shear preferentially occurred in a relatively small band of densely spaced isopycnals that were advected over a range of depths (Figs. 5d and 5e).

Patterns of dissipation reflected the changing shear field magnitude and depth structure, which was in turn controlled by the energy and evolving mode content of the wavefield (MGa). On days when shear was concentrated in a narrow vertical region (e.g., yearday 237), dissipation was concentrated as well. On other days (e.g., yeardays 238, 239, and 242) the range of high shear extended significantly below the thermocline as the proportion of shear in higher modes increased and subtidal shear became important (MGa). On both occasions the region of high dissipation rate was also more spread out (Fig. 4).

Individual profiles of dissipation, stratification and shear show dissipation to vary consistently with shear changes. For examples we turn to time periods near yearday 236.96 and yearday 238.96. Wave characteristics during these two periods were discussed in MGa (see their Figs. 7 and 11). During the first time period (Fig. 9, left panels), shear was concentrated in the thermocline, and was only comparable in magnitude to stratification in this depth range. The corresponding dissipation profile was also concentrated in the thermocline. During the second time period, the presence of elevated high-mode energy increased shear variance, especially below the thermocline (Fig. 9b). Dissipation reflected this changing shear structure, with strong patches of elevated turbulence below the thermocline (Fig. 9d).

High diffusivity may result from high dissipation and/or low stratification. Some patches of high diffusivity corresponded to relatively turbulent patches, as in the

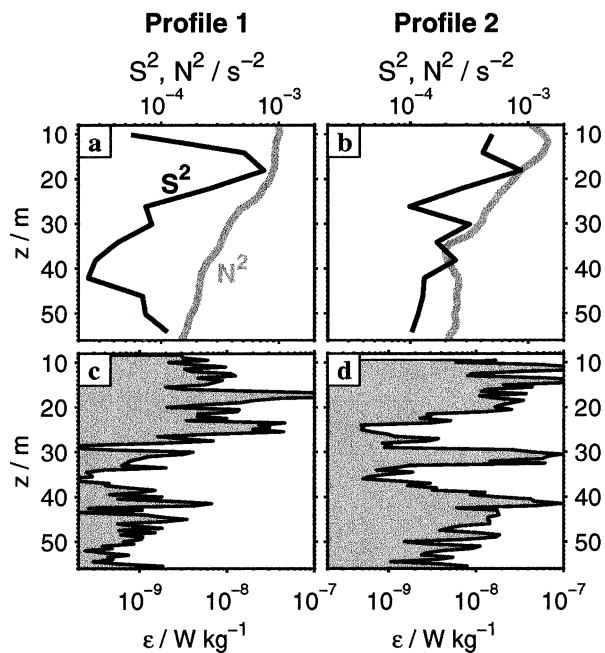


FIG. 9. (a) Average shear and stratification for a 0.5-h interval surrounding yearday 235.96. (c) Average dissipation during this time period. (b), (d) Same for interval surrounding yearday 238.96.

thermocline on yearday 238 and depth between 20 and 40 m during yearday 242 (Fig. 4). Other patches of high diffusivity were associated with anomalously low stratification but not with elevated dissipation, such as above

the bottom boundary layer on yearday 241. As many of these patches consisted of homogeneous water, high diffusivity did not result in significant turbulent fluxes.

c. Solibores

One-half of the dissipation in the thermocline and some of the largest diffusivities were observed during the passage of solibores. Of the six solibores that passed by during our microstructure profiling, the largest four (yeardays 235, 240, 241, and 242) were clearly associated with elevated dissipation in the upper water column (Fig. 4c, labeled with an “S”). The strong solibore on yearday 235 alone contributed 60% of the total solibore-related dissipation. Though solibore turbulence extended well below the thermocline (down to nearly 40 m in some cases), resultant diapycnal fluxes were acting on isopycnals that advected downward with each pulse, not the isopycnals that normally occupied this depth range (Figs. 5b and 5e).

The evolution of dissipation within the strongest solibore is shown in Fig. 10. Contours of velocity (black lines) and shear (shaded) are shown, overlaid with profiles of turbulent dissipation rate. The spacing of the dissipation profiles illustrates the degree to which our profiler undersampled the event. The locations of two reference isopycnals that bound the thermocline are shown for each profile. Average dissipation within this density range remained around $10^{-6} \text{ W kg}^{-1}$ in the third through seventh profiles (until minute 30), then de-

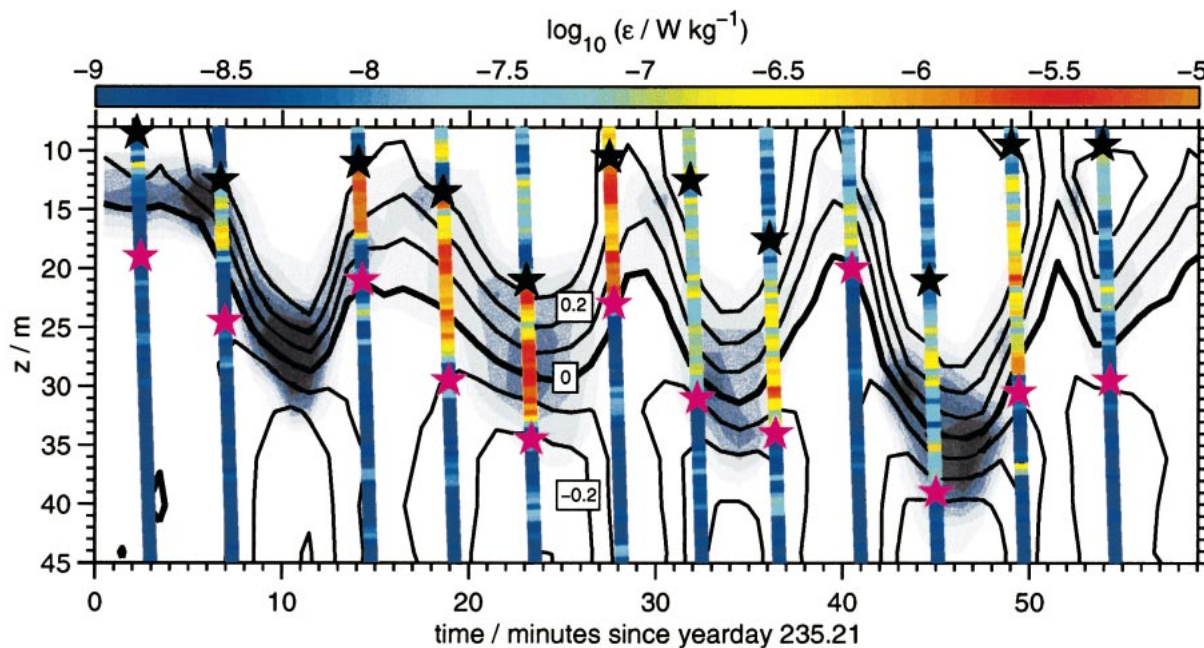


FIG. 10. The solid lines are contours of northward (onshelf) baroclinic velocity from -0.3 to 0.3 m s^{-1} in intervals of 0.1 m s^{-1} . The shaded areas are 4-m shear variance, ranging from 0 (white) to $3.5 \times 10^{-3} \text{ s}^{-2}$ (black) in increments of $5 \times 10^{-4} \text{ s}^{-2}$. Profiles of dissipation rate are overlain, and correspond to the colorbar above. The slight slant of each profile represents the passage of time as the profiler descends. The black (upper) and magenta (lower) stars on each profile indicate the evolving locations of the 22.65 and 24 kg m^{-3} isopycnals, respectively.

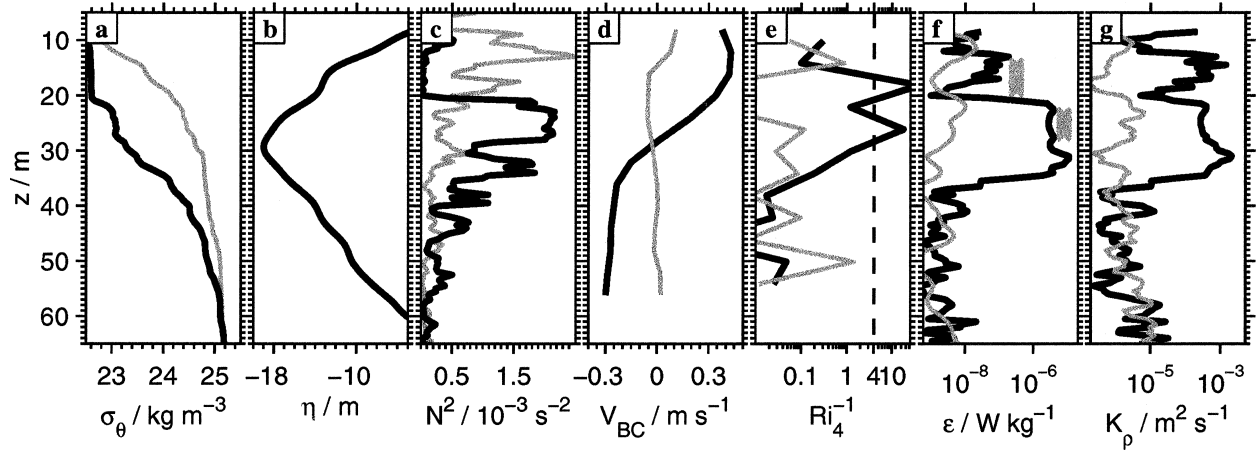


FIG. 11. Profiles of various quantities immediately before (thin, gray) and during (thick, black) the first three troughs of the yearday 235 solibore, the latter averaged isopycnally and plotted vs the depth of isopycnals at minute 22 (Fig. 10): (a) potential density, (b) isopycnal displacement between the two density profiles shown in (a), (c) buoyancy frequency, (d) northward baroclinic velocity, (e) Richardson number based on 4-m shear and stratification, (f) dissipation rate, and (g) diapycnal diffusivity.

creased an order of magnitude during the subsequent 30 minutes (six profiles).

Comparison of dissipation and shear in Fig. 10 suggests that turbulent patches were created and accentuated in the high-shear troughs of each wave pulse, then advected with isopycnals between troughs. Observed overturns in the peak dissipation patches were around 0.5 m tall, comparable to the local Ozmidov scale, $l \sim \sqrt{\epsilon/N^3}$. The associated eddy turnover time was several minutes. With wave timescales comparable to those of the overturns that they generate, the cumulative effects of shear patches may be important (Sandstrom et al. 1989; Polzin et al. 1996). For example, though dissipation in the (strongest) shear of the first wave trough (minutes 10–11) was not measured, remnants of that event were observed after it advected upward (third profile, minute 14). This patch of elevated dissipation followed isopycnals as they advected up and down through the next three wave troughs. Dissipation grew after encountering strong mode-1 shear in each trough, while gradually expanding to encompass a broader depth range. Dissipation in each profile continued to be centered on the same isopycnal range.

Profiles of turbulence within solibore troughs show elevated turbulence in two patches that roughly correspond to the depth ranges of unstable Richardson numbers (Fig. 11f). Exact comparison of depth ranges of turbulence and unstable Richardson number is hampered by the low vertical resolution of shear and the uncertainties of averaging turbulence on rapidly moving isopycnals. Perhaps a bit surprisingly, though the inverse Richardson number was larger in the higher patch (at or above 20 m), the dissipation rate was significantly larger in the lower patch (20–35 m).

When the resolved Richardson number is unstable, turbulent dissipation can be modeled using the kinematic

parameterization of Kunze et al. (1990). The average dissipation rate over the lifetime of a turbulent event is taken as the ratio of the kinetic energy loss needed to return the Richardson number to 0.25 (the threshold value for stability) and a characteristic timescale for shear instability,

$$\epsilon_{\text{KWB}} = (\Delta z)^2 \left\langle \left(\frac{S^2 - 4N^2}{24} \right) \left(\frac{S - 2N}{4} \right) \right\rangle, \quad (1)$$

where Δz is the depth range over which $Ri < 1/4$ and velocity and density are both differenced over that depth range. This parameterization roughly replicates the magnitude of observed dissipation in both patches of unstable Richardson number (Fig. 11f, gray “x”s). Interestingly, it also replicates the difference in strength of dissipation between upper and lower patches. The kinematic interpretation is that, while the inverse Richardson number is larger in the upper, strain influenced region, dissipation is stronger in the deeper, shear influenced region because there is more kinetic energy available for turbulence.

Average dissipation within solibores was more variable than the energetics of the solibores. Figure 12 shows the depth-averaged dissipation rate, averaged over the duration of each solibore event, as a function of the wave energy. The average dissipation rate within a solibore packet was a nonlinear function of packet energy (points falling along the dashed line would correspond to a linear relationship). If solibore dissipation were simply proportional to wave energy, all waves would decay at a constant rate. In these observations, however, stronger solibores not only dissipated more energy in absolute terms, they also lost their energy at a faster rate than smaller waves.

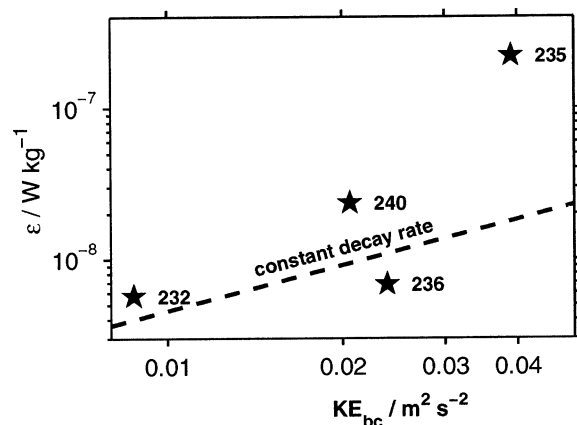


FIG. 12. Average baroclinic energy and midcolumn dissipation during the passage of the four strongest solibores, labeled with the appropriate day. The dotted line corresponds to a linear relationship.

5. Discussion I: Mechanisms of mixing

a. Hurricane Edouard

By far the strongest mixing occurred during and after the passage of Hurricane Edouard. The reduction in density range indicated a dramatic mixing event (Fig. 7). Observed stratification changes between yeardays 244 and 247 were used to estimate dissipation during the hurricane,

$$\epsilon_{\text{hur}} \sim \frac{PE_f - PE_i}{\gamma \rho \Delta t} \quad (2)$$

$$PE_{f,i} \equiv \frac{1}{h} \int_0^h \rho_{f,i} g z \, dz, \quad (3)$$

where $PE_{f,i}$ and $\rho_{f,i}$ are the final (yearday 247) and initial (yearday 244) potential energy and density of the water column, Δt is the time over which mixing occurred, h is the height of the water column (70 m), and γ is a mixing efficiency. Based on mooring data (Fig. 6), the most active overturning occurred during the first day of the hurricane, giving $\Delta t \sim 1 \text{ day} = 8.6 \times 10^4 \text{ s}$. We assumed a mixing efficiency of $\gamma = 0.2$. Using the initial and final density profiles shown in Fig. 7, we calculated a net potential energy change of $4.5 \times 10^3 \text{ J m}^{-2}$. This translates to an average hurricane dissipation rate of $4 \times 10^{-6} \text{ W kg}^{-1}$, 100 times the prehurricane average.

b. Scaling prehurricane stratified turbulent dissipation

1) TURBULENCE PARAMETERIZATIONS

We seek to parameterize turbulent dissipation in terms of physical properties (shear, stratification) that may be more easily measured or explicitly resolved by numerical simulations. Most oceanic turbulence away from frictional boundary layers is thought to be due to instabilities (primarily shear or convective) of small-ver-

tical-scale waves. This process, hereinafter referred to as wave breaking, occurs in erratic bursts on smaller scales than the ADCP can resolve. However, when dissipation rates are averaged over larger time and space scales, coherent patterns of elevated turbulence appear (sec. 4b, Fig. 4c). Observed dissipation rate was elevated in the thermocline and often mirrored patterns of elevated shear that evolved over hours and days.

There are numerous turbulence parameterizations in the literature that relate bulk averages of dissipation, shear variance, and stratification; these formulas are partly empirical and partly based upon simple analytical models of the internal wave field. One of the most enduring of these is the eikonal model of Henyey et al. (1986, hereinafter referred to as HWF), which has been successfully compared to numerical simulations by HWF and, with modification, to ocean microstructure by Gregg (1989, hereinafter G89) and Polzin et al. (1995, hereinafter P95), among others. The model is based on the fate of small-scale waves, referred to as “test waves” by HWF, propagating through velocity gradients from much larger waves. The vertical scale of test waves shrinks as they refract in the shear field until they become susceptible to instability and break. HWF propose that the flux of energy to smaller scales, as described by eikonal (ray tracing) equations, is the rate-controlling process for turbulent production. HWF, G89, and P95 all use assumed spectral properties of open-ocean wavefields to relate the rate of test wave modification, and hence dissipation, to larger-scale stratification and shear.

Here this model is modified to better correspond to observed properties of waves on the continental shelf. We caution the reader against interpreting the wave-wave interaction mechanisms discussed below too strictly, especially since there are few observational studies that investigate this type of wave dynamics on shelves. Nevertheless, the model proposed here provides a dynamic framework in which to interpret simple functional relationships between variables, and is a natural extension of earlier parameterization work. As HWF argue, we justify our model less by the rigor of its assumptions than by its simple intuitive appeal and persuasive comparison with data.

Formally, following HWF and P95 we equate the turbulent dissipation rate with the spectral transfer of energy to higher vertical wavenumbers (smaller scales), using simple ray-tracing equations (Gill 1982; HWF). In the notation of P95,

$$\epsilon = \left\langle \frac{d\hat{E}}{dt} \right\rangle = \left\langle \frac{d\hat{E}}{dm} \frac{dm}{dt} \right\rangle \quad (\text{W kg}^{-1}) \quad (4)$$

$$= \left\langle \frac{d\hat{E}}{dm} \left(-\frac{dU}{dz} \cdot \mathbf{k} \right) \right\rangle \quad (\text{W kg}^{-1}), \quad (5)$$

where m is the vertical wavenumber, $\hat{E}(m)$ is the spectral energy density evaluated at some suitably high wave-

number (characterizing the energy of test waves), $\mathbf{U}(z)$ is the background velocity vector from larger-scale waves, and \mathbf{k} is the wavenumber vector of the test wave. The brackets indicate an average over time- and space scales of interest, which in our case are of order 1 h and 8 m. Neglecting the vertical component of background wave velocity, assuming the test wave energy is not correlated with background shear, and taking an rms form of (5), we have

$$\epsilon \approx \left\langle \frac{d\hat{E}}{dm} \right\rangle \left| \frac{dU}{dz} \right| k_H \quad (\text{W kg}^{-1}). \quad (6)$$

The three factors on the rhs of (6) are related to the energy density of the test waves (local derivative of spectral density), the rms background shear (from larger waves), and the horizontal wavenumber of the test waves, respectively.

Open-ocean turbulence parameterizations then make several assumptions about the nature of the internal waves. Most important to this discussion, they assume that the waves are in a statistically steady state in which the (rms) energy of small-scale waves and the (rms) shear of the larger-scale waves maintain a particular relationship through a prescribed spectral shape. This spectral shape is taken to be either the Garrett–Munk (GM) spectrum (HWF), or a close relative with slightly modified wavenumber or frequency properties (P95). This distribution of waves is assumed to slowly evolve with changes in stratification and total wavefield energy such that the vertical wavenumber of test waves depends only on the spectral energy level. Specifically, it is chosen such that the Froude spectra integrated out to a near-breaking wavenumber is order 1. Plugging in the analytical form of the GM spectrum and the dispersion relationship, the three factors on the rhs of (6) can be related to each other in such a way that at a particular latitude the dissipation rate scales as

$$\epsilon \propto f \hat{E}^2 \left(\frac{N^2}{N_0^2} \right) \quad (\text{W kg}^{-1}), \quad (7)$$

where N_0 is a reference buoyancy frequency and f is the Coriolis frequency (G89).

To compare this scaling with oceanic measurements at a variety of midlatitude locations, G89 uses the ratio of measured shear at a fixed wavenumber (10 m) to the modeled Garrett–Munk shear at that scale as a proxy for the spectral energy level to get what we will subsequently refer to as the Gregg–Heney (G–H) scaling,

$$\epsilon_{\text{GH}} = 1.8 \times 10^{-6} \left[f \cosh^{-1} \left(\frac{N_0}{f} \right) \right] \left(\frac{S_{10}^4}{S_{\text{GM}}^4} \right) \left(\frac{N^2}{N_0^2} \right) \quad (8)$$

$$S_{\text{GM}}^4 = 1.66 \times 10^{-10} \left(\frac{N^2}{N_0^2} \right)^2. \quad (9)$$

To adapt the HWF analytical model to the shelf, we

incorporate wave properties observed by MGa. In particular, we note that large-scale (low mode) shear was primarily from low-frequency waves whose energy and relative modal content varied considerably from day to day. Much of the low-frequency shear was from the internal tide, which is not included in GM-type spectral models. Furthermore, the energy of the highest modes resolved here did not maintain any consistent relationship with the rms magnitude of low-mode shear. We therefore cannot assume the type of relationships between the terms of (6) employed by HWF and P95. Instead we make several simpler propositions.

- 1) The large-scale shear that provides the environment for test waves comes primarily from near-inertial and semidiurnal waves. We thus use low-frequency shear in (6), denoted by S_{lf} . This choice is appealing not only because it produces the most successful comparison with data, but also because narrowband waves may be easier to explicitly model or observe.
- 2) The energy density of the test waves is beyond our ability to reliably measure, but we assume it scales with stratification in a Wentzel–Kramers–Brillouin (WKB) sense (Gill 1982). Beyond this, properties of small-scale waves cannot be simply related to observed variables; hence typical test wave energy density (E_0) and vertical wavenumber (m_0) are treated as unknown constants.
- 3) The wavenumber of the test waves also cannot be simply related to observed large-scale motions. According to WKB theory, horizontal wavenumber (k_H) does not change in a stratification field that only varies in the vertical. We therefore also treat the characteristic horizontal wavenumber in (6) as an unknown constant.

With these assumptions, the three terms in (6) scale as

$$\left\langle \frac{d\hat{E}}{dm} \right\rangle \propto \frac{E_0}{m_0} \left(\frac{N}{N_0} \right) \quad (10)$$

$$\sqrt{\left(\frac{dU}{dz} \right)^2} \propto S_0 \left(\frac{S_{lf}}{S_0} \right) \quad (11)$$

$$k_H \propto k_{H0}. \quad (12)$$

The product of all three terms gives a dissipation rate estimate that we will refer to as the MacKinnon–Gregg (M–G) scaling

$$\epsilon_{\text{MG}} = \epsilon_0 \left(\frac{N}{N_0} \right) \left(\frac{S_{lf}}{S_0} \right) \quad (\text{W kg}^{-1}) \quad (13)$$

where ϵ_0 combines the dimensional terms in (10)–(12). We set $N_0 = S_0 = 3$ cph for simplicity. We choose $\epsilon_0 = 6.9 \times 10^{-10}$ to give the modeled dissipation rate the same cruise-average as the observed data. We expect uncertainties in the wavenumber and energy density of small-scale waves (beyond WKB scaling) to create a substantial amount of scatter between the modeled and

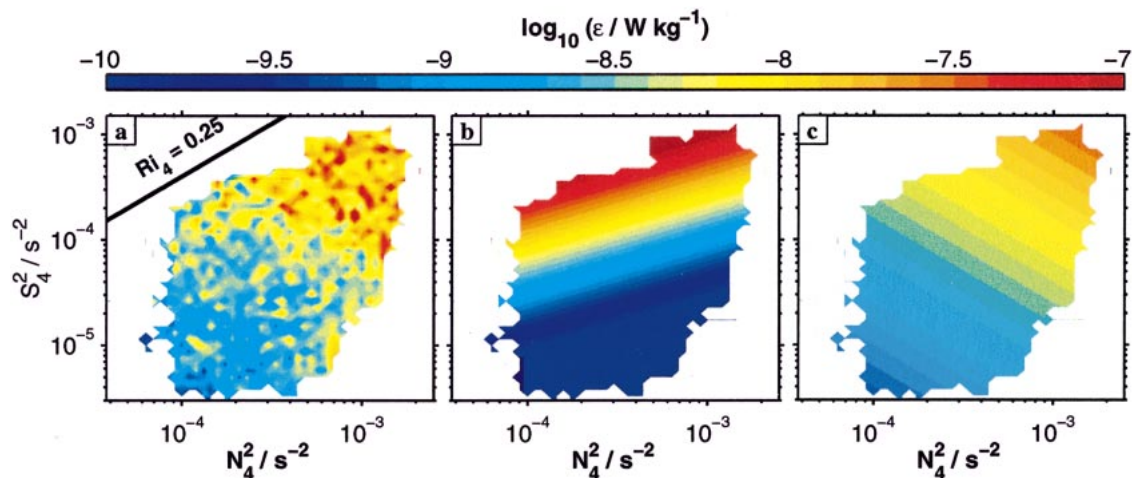


FIG. 13. (a) Observed dissipation data averaged in bins of 4-m stratification (x axis) and 4-m shear variance (y axis). The boundary of 4-m Richardson number = 0.25 is shown for reference. (b), (c) Same as for the the Gregg–Heney and MacKinnon–Gregg parameterizations, respectively.

observed dissipation rate. Nevertheless, the shear and stratification scaling of the two parameterizations, (8) and (13), are substantially different and we should be able to use our data to differentiate between them.

2) COMPARING DISSIPATION PARAMETERIZATIONS TO DATA

We compare observed CMO dissipation rates with both the G–H and the M–G parameterizations and conclude that, while both capture the shape of the average dissipation rate profile, the new parameterization is much better at reproducing dissipation rate variability. To compare both parameterizations with the data, we created two model dissipation datasets based upon (8) and (13). For consistency we used 4-m low-frequency shear in both parameterizations (instead of S_{10}), though the results are not sensitive to this choice. Both modeled and observed data were smoothed using an 8-m Bartlett filter to be consistent with the ADCP shear resolution. Modeled and observed data are compared in several ways below. All data inside of or within 3 m of surface or bottom mixed layers has been excluded.

(i) Joint shear and stratification dependence

To evaluate the success of either model in reproducing the variability of dissipation, we consider kinematic relationships between shear variance, stratification, and dissipation rate (real and modeled). We compute averages of all three dissipation datasets in logarithmically evenly spaced bins of shear and stratification (Fig. 13). Only bins that contain at least five dissipation values are presented. Both the real data and the M–G modeled dissipation rate increase with increasing stratification and increasing shear (from bottom left to top right). The total range of M–G model dissipation rates is comparable to that of the observed data. In contrast, the G–

H model dissipation rate has an inverse relationship with stratification, and a much larger range of values than the real data. We find the simple but striking visual differences between these plots the most persuasive argument in favor of a new model of turbulent dissipation. Solibores are not included in this section, primarily because not enough data was collected during solibore events to perform two-dimensional binning.

(ii) Separate shear and stratification dependence

Next, we wish to evaluate to what extent either shear or stratification by itself can be used as a reliable proxy for dissipation rate and, if so, to characterize the relationship. Figure 14 shows dissipation rate and diffusivity binned in terms of stratification or shear alone. These are equivalent to integrating the two-dimensional plots in Fig. 13 horizontally and vertically.

The clearest difference between the real and model datasets is in the shear dependency (Figs. 14a,c). The M–G model effectively reproduces the slope of the dissipation rate versus shear and diffusivity versus shear relationships. The G–H model dissipation has a much steeper relationship with shear. Both models capture the essential kinematic relationship between dissipation rate and stratification (Figs. 14b,d). The G–H model is too large on average, but otherwise both models reproduce the change between $\epsilon \propto N^0$ for $N \leq 2 \times 10^{-4} \text{ s}^{-1}$ and $\epsilon \propto N^2$ for larger stratification.

The slopes shown in Fig. 14 are not the simple linear plots that one might expect from the scaling in (13) because shear and stratification are not independent variables; in other words, the one-dimensional integrated versions of Fig. 13 reflect the shape of the kinematic domain of observed data. In strongly stratified regions ($N \geq 2 \times 10^{-4} \text{ s}^{-2}$), shear and stratification are well correlated and have a nearly linear relationship; thus the

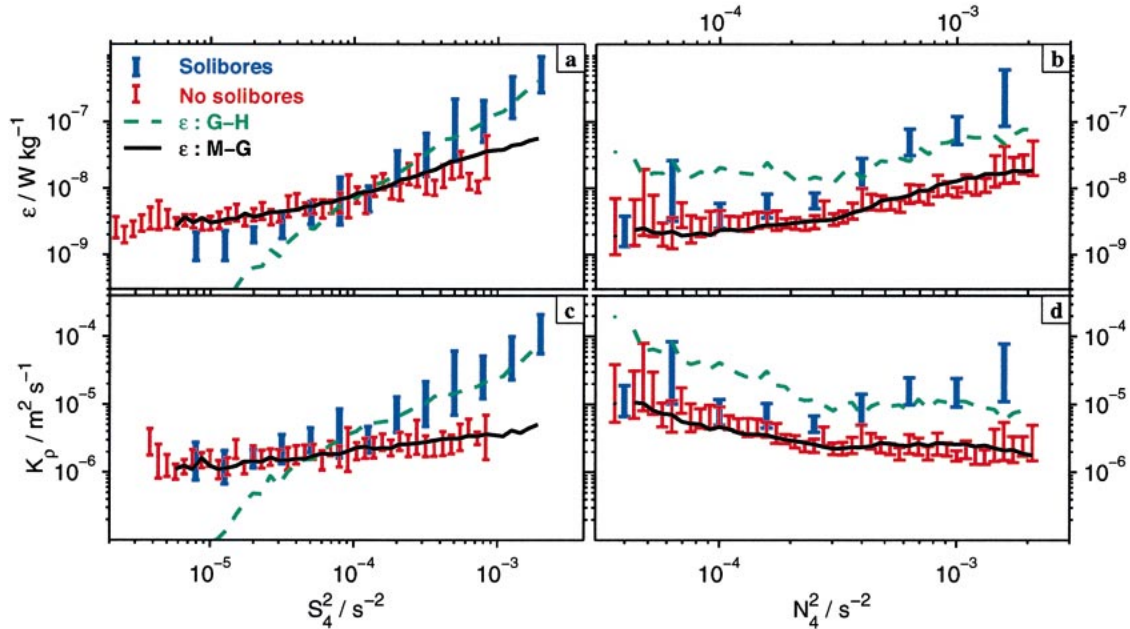


FIG. 14. (a), (b) The average turbulent dissipation rate calculated in bins of stratification and shear. (c), (d) Average diffusivity in bins of stratification and shear. In all panels measured dissipation rates during and excluding solibores are represented by the thick blue and thinner red bars respectively. The height of each bar is a bootstrap 95% confidence interval. Gregg–Henyey and MacKinnon–Gregg model dissipation fields averaged in the same manner are represented by the dashed green and thick black lines, respectively.

scaling (13) appears as $\epsilon \propto N^2$ (Fig. 14b), leading to a flat diffusivity (Fig. 14d). On the other hand, there were also many patches of low stratification. These patches tend not to be large enough to significantly change the shapes of low modes and, hence, do not significantly affect low-mode shear. Within these patches (generally represented by the $N \leq 2 \times 10^{-4} \text{ s}^{-2}$ portions of Figs.

14b,d), stratification and shear were not correlated; thus diffusivity scales inversely with stratification. Similar ideas were recently presented by Duda and Rehmann (2002).

Ironically, the G–H model agrees quite well with the dissipation during solibores (blue bars). This agreement may be coincidental; we suggest that the steeper dissipation versus shear relationship during the solibores is not due to the increased applicability of the assumptions behind G–H, but rather the fact that during solibores the first-mode shear was often in itself large enough to push Richardson numbers below critical, invalidating the assumptions of both models. In particular, dissipation scales as the third power of shear in the successful kinematic scaling of Kunze et al. (1990) (1), which may account for the steep slope of the blue bars in Fig. 14.

(iii) Comparing average profiles

Last, we compare average profiles of dissipation rate based on observed data (with and without solibores) and the two models (Fig. 15). In all cases, average dissipation rate decreased between 10 and 40 m, mirroring declines in both shear and stratification. Both parameterizations roughly have the right shape, though the G–H profile is too large by a factor of 3–5. Averaged over a fortnight, shear scaled roughly with average stratification ($S^2 \propto N^2$), which collapses both scalings to form similar average profiles.

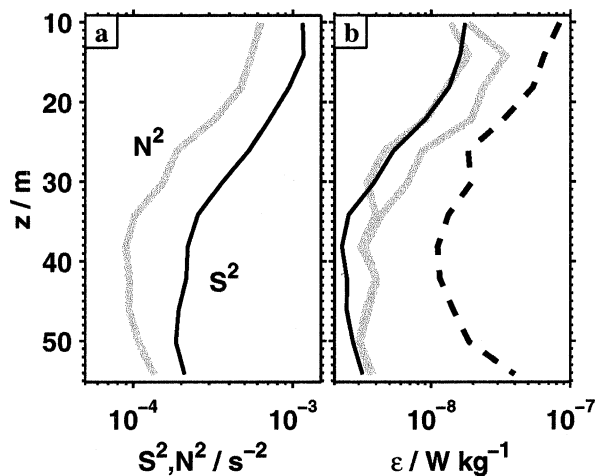


FIG. 15. (a) Prehurricane averaged profiles of shear and stratification at 4-m resolution. (b) Average profiles of dissipation rate with and without solibores (thick, gray), and average model dissipation rate based on Gregg–Henyey (dashed) and MacKinnon–Gregg (thin, black) parameterizations.

3) PARAMETERIZATION APPLICABILITY

The extent to which the new parameterization proposed here is applicable in other circumstances is a major open question. We expect scalings along these lines may be appropriate in locations and seasons where and when turbulence is primarily due to internal wave instability (as opposed to boundary mixing), and the shear from low-frequency, low-mode waves is not related to the energy of higher-mode waves through any particular steady spectral shape. MacKinnon and Gregg (2003b, manuscript submitted to *J. Phys. Oceanogr.*) find that turbulence on the CMO shelf in the late spring of 1997 follows the same parameterization proposed here, albeit with a slightly different value of the dimensional scaling parameter ϵ_0 . In general, ϵ_0 represents characteristic energy levels and lengthscales of test waves, and may be sensitive to the details of high wavenumber wave generation. Future observations in this and other environments that explicitly resolved smaller velocity scales, and appropriate scale numerical modeling would be immensely helpful towards resolving these questions.

6. Discussion II: Context and effects of turbulence

a. Comparison with other results

Among the suite of CMO mixing measurements, results presented here compare most favorably with the dye-release experiments of Sundermeyer and Ledwell (2001). In September 1995, they injected dye onto $\sigma_\theta = 25.2 \text{ kg m}^{-3}$ at depth 45 m and observed a diffusivity of $1.5 \times 10^{-5} \text{ m}^2 \text{ s}^{-1}$. In August of 1997, they found diffusivity on the 24.6 isopycnal at 20-m depth to be $2.5 \times 10^{-6} \text{ m}^2 \text{ s}^{-1}$. The agreement with our data (Fig. 5) is remarkable, especially considering the variability of shelf mixing and the three years separating the measurements. Rehmann and Duda (2000) measured conductivity microstructure in the CMO area in August 1997 and estimated average midcolumn thermal diffusivity to be 2–5 ($\times 10^{-5} \text{ m}^2 \text{ s}^{-1}$), a value 2–10-fold greater than our results. Though they find some evidence of double-diffusive processes, the largest diffusivities they observed were in diffusively stable water with low stratification, consistent with our results. In general, it is difficult for us to distinguish the possible role of double diffusive processes from internal wave or frictional shear instabilities in mixing. The water column was generally double-diffusively stable except near the bottom and during strong intrusions on yeardays 238 and 248. In both cases strong shear related turbulence was also present.

b. Diffusion

Measured diffusivity was comparable in magnitude to observed water property changes only after the hurricane. After the storm passed the density range in the lower water column continued to drop over several days

[sec. 3b(2) Figs. 6 and 7). Average diffusivity in the stratified interface approximately 10 m tall was 5–10 ($\times 10^{-4} \text{ m}^2 \text{ s}^{-1}$). Based on a simple Fickian scaling analysis, $T \propto L^2/K_\rho$, the timescale for significant diffusive change should be a few days, comparable to the observed warming rate of the bottom layer (Fig. 6).

Specific diffusive changes were obscured by advection during the rest of our observations. Not only did water property changes have definitive signatures of advection (sec. 3b), but the typical timescales of water change were too large to be explained by observed diffusivities. An average midcolumn diffusivity of $5 \times 10^{-6} \text{ m}^2 \text{ s}^{-1}$ would take months to affect a 5-m feature based upon Fickian scaling. However, the high diffusivity within some solibores ($10^{-3} \text{ m}^2 \text{ s}^{-1}$) could affect 5-m features in less than a day or 1-m features in an hour or less. Once again, we were unable to detect definitive evidence of solibore mixing due to constant advective changes on these time and spatial scales.

Though simple one-dimensional mixing models may not be appropriate most of the time, the measurements presented here may be important for understanding long timescale and large spatial-scale fluxes across isopycnals and associated hydrographic changes. Most isopycnals below the thermocline extended through a variety of dynamic regimes. A net flux of water mass or tracer substance into a given portion of an isopycnal layer can either occur through a local diapycnal flux convergence or through a diapycnal flux convergence elsewhere that is isopycnally mixed through the density layer (Sundermeyer and Ledwell 2001). For increasing distance offshore, each isopycnal was progressively in the bottom boundary layer, above the boundary layer, and close to the thermocline. Diapycnal fluxes into these isopycnal layers may occur anywhere along the way, by any of the processes presented here.

c. Energetics

Midcolumn dissipation was a strong drain on the internal wave field and of first-order importance for the energetics of solibores and higher-mode internal waves. Local dissipation played a relatively important role in internal wave dynamics. One measure of the impact of dissipation is the timescale for complete decay of the internal wave field. Based on the observed depth-averaged energy density, $6.3 \times 10^{-3} \text{ J kg}^{-1}$, and average dissipation rate away from boundaries, $10^{-8} \text{ W kg}^{-1}$, the baroclinic energy would be completely drained in 7 days. For comparison, in a Garrett–Munk open ocean thermocline with standard stratification ($N_0 = 3 \text{ cph}$), the energy density is one-half of that observed in CMO, but typical dissipation rates are over an order of magnitude lower, leading to a decay timescale of 50 days. Further implications of dissipation on internal wave dynamics are discussed in MGA.

7. Conclusions

The major results of this study can be summarized as follows:

- Midcolumn dissipation and diffusivity on the stratified summer shelf were fairly weak, $5\text{--}50 (\times 10^{-9} \text{ W kg}^{-1})$ and $5\text{--}20 (\times 10^{-6} \text{ m}^2 \text{ s}^{-1})$, comparable to the open ocean thermocline and too low to explain strong variability observed in local water properties. Nevertheless, observed turbulence is dynamically interesting and essential for understanding diffusion throughout the thermocline on longer timescales.
- Dissipation and associated diapycnal fluxes displayed significant variability. Dissipation in the bottom boundary layer varied with the near-bottom flow. One-half the thermocline dissipation was from four solibores, which cumulatively lasted less than a day but contained 100-fold elevated dissipation and diffusivity. The role of such strong episodic events, especially important for diffusion on scales less than 5 m, cannot be well captured by average dissipation profiles. On a shelf with sloping isopycnals, both diapycnal and isopycnal diffusion play a role in net cross-isopycnal fluxes.
- Midcolumn dissipation was well correlated with local shear variance, both in an average and fluctuating sense. The Gregg–Heneyy dissipation parameterization does not capture the variability of observed turbulence. For nonsolibore periods, we propose an alternate model (13) based on the simple kinematic model of Heneyy et al. (1986), modified for an environment where large- and small-scale waves may not maintain a steady spectral relationship. The new parameterization agrees well with observed turbulent dissipation. This parameterization is based on estimates of stratification and shear from low-frequency deterministic waves, both of which may be comparatively easy to measure or explicitly include in a numerical model.
- During the solibores the mode-1 shear produced unstable Richardson numbers, and no parameterization based on wave–wave interactions is likely to be appropriate. The best hope for modeling this strong and important turbulence may be kinematic scalings such as (1).
- The passage of Hurricane Edouard produced a 100-fold increase in average dissipation during the peak of the storm ($4 \times 10^{-6} \text{ W kg}^{-1}$). Mixing of the top portion of the water column was fairly complete and occurred during the storm passage. Significant mixing of the lower water continued for several days after the storm and was consistent in magnitude with observed frictional dissipation associated with the large along-shelf flow after the storm. Hurricane mixing may be best viewed as the first event of a mixing regime dominated by winter storms rather than as a feature of stratified summer mixing.

Acknowledgments. We thank Jody Klymak, Earl Krause, Jack Miller, Gordon Welsh, and the entire crew of the R/V *Seward Johnson* for help with data collection. Numerous other CMO investigators generously shared their thoughts and results with us. We thank in particular Wilf Gardner, Murray Levine, Tim Boyd, Jack Barth, Steve Anderson, James Edson, Al Plueddemann, Steve Lentz, Steven Babin, and Ray Sterner. The comments of an anonymous reviewer were quite helpful in improving the clarity of our analysis. This work was supported by ONR Grant N00014-95-1-0406. Jennifer MacKinnon received additional support from an NDSEG research fellowship. Michael Gregg received additional support from the SECNAV/CNO Chair in Oceanography.

REFERENCES

- Alford, M., and R. Pinkel, 2000: Observations of overturning in the thermocline: The context of ocean mixing. *J. Phys. Oceanogr.*, **30**, 805–832.
- Barth, J. A., D. Bogucki, S. D. Pierce, and P. M. Kosro, 1998: Secondary circulation associated with a shelfbreak front. *Geophys. Res. Lett.*, **25**, 2761–2764.
- Chapman, D. C., and R. C. Beardsley, 1989: On the origin of shelf water in the Middle Atlantic Bight. *J. Phys. Oceanogr.*, **19**, 384–391.
- Dickey, T., G. Chang, Y. Agrawal, A. Williams III, and P. Hill, 1998: Sediment resuspension in the wakes of hurricanes Edouard and Hortense. *Geophys. Res. Lett.*, **25**, 3533–3536.
- Duda, T., and C. Rehmann, 2002: Systematic microstructure variability in double diffusively stable coastal waters of nonuniform density gradient. *J. Geophys. Res.*, **107**, 3144, doi:10.1029/2001JC000844.
- Gardner, W., and Coauthors, 2001: Optics, particles, stratification, and storms on the New England continental shelf. *J. Geophys. Res.*, **106**, 9473–9497.
- Gill, A. E., 1982: *Atmosphere–Ocean Dynamics*. Academic Press, 662 pp.
- Gregg, M. C., 1989: Scaling turbulent dissipation in the thermocline. *J. Geophys. Res.*, **94**, 9686–9698.
- , 1998: Estimation and geography of diapycnal mixing in the stratified ocean. *Physical Processes in Lakes and Oceans*, J. Imberger, Ed., Coastal and Estuarine Studies, American Geophysical Union, 305–338.
- Heneyy, F. S., and A. Hoering, 1997: Energetics of borelike internal waves. *J. Geophys. Res.*, **102**, 3323–3330.
- , J. Wright, and S. M. Flatté, 1986: Energy and action flow through the internal wave field. *J. Geophys. Res.*, **91**, 8487–8495.
- Houghton, R. W., R. Schlitz, R. C. Beardsley, B. Butman, and J. L. Chamberlin, 1982: The Middle Atlantic Bight cold pool: Evolution of the temperature structure during summer 1979. *J. Phys. Oceanogr.*, **12**, 1019–1029.
- Inall, M. E., T. P. Rippeth, and T. J. Sherwin, 2000: The impact of non-linear waves on the dissipation of internal tidal energy at a shelf break. *J. Geophys. Res.*, **105**, 8687–8705.
- Kunze, E., A. Williams III, and M. G. Briscoe, 1990: Observations of shear and vertical stability from a neutrally buoyant float. *J. Geophys. Res.*, **95**, 18 127–18 142.
- Ledwell, J., A. Watson, and C. Law, 1993: Evidence for slow mixing across the pycnocline from an open-ocean tracer-release experiment. *Nature*, **364**, 701–703.
- Linder, C. A., and G. Gawarkiewicz, 1998: A climatology of the shelfbreak front in the Middle Atlantic Bight. *J. Geophys. Res.*, **103**, 18 405–18 423.

- MacKinnon, J., and M. Gregg, 2003a: Shear and baroclinic energy flux on the summer New England shelf. *J. Phys. Oceanogr.*, **33**, 1462–1475.
- Nash, J. D., and J. N. Moum, 2001: Internal hydraulic flows on the continental shelf: High drag states over a small bank. *J. Geophys. Res.*, **106**, 4593–4612.
- Oakey, N. S., 1982: Determination of the rate of dissipation of turbulent energy from simultaneous temperature and velocity shear microstructure measurements. *J. Phys. Oceanogr.*, **12**, 256–271.
- O'Malley, R., J. Barth, A. Erofeev, J. Fleischbein, P. Kosro, and S. Pierce, 1997: Seasoar CTD observations during the Coastal Mixing and Optics experiment. Tech. Rep. Data Rep. 168, College of Oceanic and Atmospheric Sciences, Oregon State University.
- Osborn, T. R., 1980: Estimates of the local rate of vertical diffusion from dissipation measurements. *J. Phys. Oceanogr.*, **10**, 83–89.
- Polzin, K. L., J. M. Toole, and R. W. Schmitt, 1995: Finescale parameterizations of turbulent dissipation. *J. Phys. Oceanogr.*, **25**, 306–328.
- , N. S. Oakey, J. M. Toole, and R. W. Schmitt, 1996: Fine structure and microstructure characteristics across the northwest Atlantic subtropical front. *J. Geophys. Res.*, **101**, 14 111–14 121.
- Rehmann, C. R., and T. F. Duda, 2000: Diapycnal diffusivity inferred from scalar microstructure measurements near the New England shelf/slope front. *J. Phys. Oceanogr.*, **30**, 1354–1371.
- Rippeth, T. P., and M. E. Inall, 2002: Observations of the internal tide and associated mixing across the Malin shelf. *J. Geophys. Res.*, **107**, 3028, doi:10.1029/2000JC000761.
- Sandstrom, H., and J. Elliott, 1984: Internal tide and solitons on the Scotian shelf: A nutrient pump at work. *J. Geophys. Res.*, **89**, 6415–6426.
- , and N. Oakey, 1995: Dissipation in internal tides and solitary waves. *J. Phys. Oceanogr.*, **25**, 604–614.
- , J. Elliott, and N. Cochrane, 1989: Observing groups of solitary internal waves and turbulence with batfish and echo-sounder. *J. Phys. Oceanogr.*, **19**, 987–997.
- Simpson, J. H., W. R. Crawford, T. Rippeth, A. Campbell, and J. Cheok, 1996: The vertical structure of turbulent dissipation in shelf seas. *J. Phys. Oceanogr.*, **26**, 1579–1590.
- , T. Rippeth, and A. Campbell, 2000: The phase lag of turbulent dissipation in tidal flow. *Interactions between Estuaries, Coastal Seas and Shelf Seas*, T. Yanagi, Ed., Terra Scientific, 57–67.
- Sundermeyer, M., and J. Ledwell, 2001: Lateral dispersion over the continental shelf: Analysis of dye-release experiments. *J. Geophys. Res.*, **105**, 9603–9621.
- Voorhis, A., D. Webb, and R. Millard, 1976: Current structure and mixing in the shelf/slope water front south of New England. *J. Geophys. Res.*, **81**, 3695–3707.
- Wesson, J. C., and M. C. Gregg, 1994: Mixing at Camarinal Sill in the Strait of Gibraltar. *J. Geophys. Res.*, **99**, 9847–9878.
- Wijesekera, H., L. Padman, T. Dillon, M. Levine, and C. Paulson, 1993: The application of internal-wave dissipation models to a region of strong mixing. *J. Phys. Oceanogr.*, **23**, 269–286.